ACCEPTED MANUSCRIPT

BASIS FOR THE ICRP'S UPDATED BIOKINETIC MODEL FOR SYSTEMIC ASTATINE

Rich Leggett and Caleigh Samuels
Environmental Sciences Division
Oak Ridge National Laboratory
P.O. Box 2008
Oak Ridge, TN 37831

This manuscript has been authored by UT-Battelle, LLC under Contract No. DE-AC05-00OR22725 with the US Department of Energy. The United States Government retains and the publisher, by accepting the article for publication, acknowledges that the United States Government retains a non-exclusive, paid-up, irrevocable, world-wide license to publish or reproduce the published form of this manuscript, or allow others to do so, for United States Government purposes. The Department of Energy will provide public access to these results of federally sponsored research in accordance with the DOE Public Access Plan (http://energy.gov/downloads/doe-public-access-plan).

The work described in this manuscript was sponsored by the Office of Radiation and Indoor Air, U. S. Environmental Protection Agency (EPA), under Interagency Agreement DOE No. 1824 S581-A1, under contract No. DE-AC05-00OR22725 with UT-Battelle.

BASIS FOR THE ICRP'S UPDATED BIOKINETIC MODEL FOR SYSTEMIC ASTATINE

Rich Leggett and Caleigh Samuels

Abstract

The ICRP recently updated its biokinetic models for workers in a series of reports called the OIR (Occupational Intakes of Radionuclides) series. A new biokinetic model for astatine, the heaviest member of the halogen family, was adopted in OIR Part 5 (ICRP Publication 151, in press). This paper provides an overview of available biokinetic data for astatine; describes the basis for the ICRP's updated model for astatine; and tabulates dose coefficients for intravenous injection of each of the two longest lived and most important astatine isotopes, ^{211}At and ^{210}At. Astatine-211 ($T_{1/2}$ = 7.214 h) is a promising radionuclide for use in targeted α-particle therapy due to several favorable properties including its half-life and the absence of progeny that could deliver significant radiation doses outside the region of α-particle therapy. Astatine-210 ($T_{1/2}$ = 8.1 h) is an impurity generated in the production of ^{211}At in a cyclotron and represents a potential radiation hazard via its long-lived progeny ^{210}Po ($T_{1/2}$ = 138 d). Tissue dose coefficients for injected ^{210}At and ^{211}At based on the updated model are shown to differ considerably from values based on the ICRP's previous model for astatine, particularly for the thyroid, stomach wall, salivary glands, lungs, spleen, and kidneys.

Introduction

Astatine (At) is the heaviest member of the halogen group of elements (Group VIIA). Its name comes from the Greek word *astatos*, meaning unstable. The existence of astatine had been predicted since the 1800s but was not firmly established until 1940 when ^{211}At ($T_{1/2}$ = 7.214 h) was produced in a cyclotron at the University of California by alpha particle bombardment of bismuth-209 (^{209}Bi). Dozens of other short-lived radioisotopes of astatine have since been identified or hypothesized. Due to the lack of stable or long-lived astatine, many of the chemical and physical properties of astatine have not yet been determined and are inferred from properties of other halogens (Wilbur 2013, Lindegren et al. 2020).

Publication 107 of the International Commission on Radiological Protection (ICRP 2008) provides nuclear decay data for 14 astatine isotopes (Table 1). All emit alpha particles although alpha decay is the primary mode of decay for only 5 of the 14: ^{215}At, ^{216}At, ^{217}At, ^{218}At, and ^{219}At. Astatine-211 is a promising radionuclide for use in targeted α-particle therapy due to several favorable properties including: a half-life that is sufficiently short for treatment at a high dose rate but long enough to allow offsite production and facilitate handling; it can often be incorporated into biomolecules of interest by adapting radioiodine chemistry; one decay of ^{211}At results in one alpha emission from ^{211}At either directly (41.8% of decays) or from decay of its short-lived progeny ^{211}Po (58.2%); and its only other radioactive progeny, ^{207}Bi, is a long-lived beta-gamma emitter that is not considered a significant health risk at therapeutic levels of ^{211}At administration (Vaidyanathan and Zalutsky 2008, Lindegren et al. 2020).

The longest-lived astatine isotope, ^{210}At, is not suitable for medical applications because it decays to the hazardous alpha emitter ^{210}Po ($T_{1/2}$ = 138 d). In the production of ^{211}At in a cyclotron, beam energies are set to limit production of ^{210}At to a tolerable level while producing sufficient ^{211}At for the intended application. Other modes of production of ^{211}At are feasible including production of its parent ^{211}Rn ($T_{1/2}$ = 14.6 h) (Crawford 2016), which provides a longer-lived source of ^{211}At, but cyclotron production remains the most practical method of production.

The ICRP has recently updated its biokinetic models for workers in a series of reports called the OIR (Occupational Intakes of Radionuclides) series. Astatine is addressed in OIR Part 5 (ICRP Publication 151, in press). This paper describes the basis for the ICRP's updated model for systemic astatine and, for each of the longest-lived astatine isotopes, ^{210}At and ^{211}At, compares dose coefficients based on the updated model with values based on the ICRP's previous systemic model for occupational intake of astatine (ICRP 1981, 1994).

Table 1. Properties of astatine isotopes addressed in ICRP Publication 107 (2008)			
Isotope	Half-life[a]	Decay mode[b]	% α decays[c]
At-204	9.2 m	EC, β+, α	3.8
At-205	26.2 m	EC, β+, α	10
At-206	30.6 m	EC, β+, α	0.89
At-207	1.80 h	EC, β+, α	8.6
At-208	1.63 h	EC, β+, α	0.55
At-209	5.41 h	EC, β+, α	4.1
At-210	8.1 h	EC, β+, α	0.175
At-211	7.214 h	EC, α	41.8
At-215	0.0001 s	α	100
At-216	0.0003 s	α	100
At-217	0.0323 s	α	99.99
At-218	1.5 s	α, β-	99.9
At-219	56 s	α	97
At-220	3.71 m	β-, α	8.0
[a]s = second, m = minute, h = hour [b]EC = electron capture, α = alpha decay, β+ = positive beta decay, β- = negative beta decay [c]Not including α decays from progeny			

Methods

It has been established in animal studies that the biokinetics of astatine administered intravenously as astatide initially resembles that of the next heaviest halogen, iodine, administered as iodide. Notable differences between astatine and iodide are evident within a few hours after administration, however, including lower accumulation of astatine in the thyroid and greater accumulation of astatine in extrathyroidal tissues, particularly phagocytic tissues (i.e., with relatively high levels of macrophages) such as spleen, liver, and lung (Hamilton et al., 1953; Brown, 1986; Garg et al., 1990).

The model for systemic astatine described in this paper reflects a variety of sources of biokinetic data for astatine collected in a review of the literature but is based to a large extent on comparison and contrast with the systemic kinetics of iodide. The starting place for the astatine model is the ICRP's biokinetic model for iodide (I^-), which is one of three subsystems comprising the ICRP's current model for systemic iodine (ICRP 2017): (1) iodide kinetics, (2) thyroidal trapping of iodide and subsequent production, storage, and release of the thyroid hormones T_3 and T_4; and (3) extrathyroidal T_3 and T_4 kinetics including recycling of released iodide to blood. The model for the iodide subsystem is shown in Figure 1. The shaded boxes representing the other two subsystems of the ICRP's iodine model do not represent iodide kinetics per se but are included to indicate that iodide converted to organic iodide is largely recycled over time to the blood iodide pool.

The model for astatine was constructed in large part by modifying transfer rates in the iodide model to reflect the observed differences in the biokinetics of astatine and iodide in laboratory animals, although more direct use is made of some data sets for astatine including data for human subjects. Some changes in the model structure for iodide were made to address the observed elevated uptake of astatine by phagocytic tissues and to simplify the model for Other tissue shown in Figure 1 in view of the limited information on the kinetics of astatine.

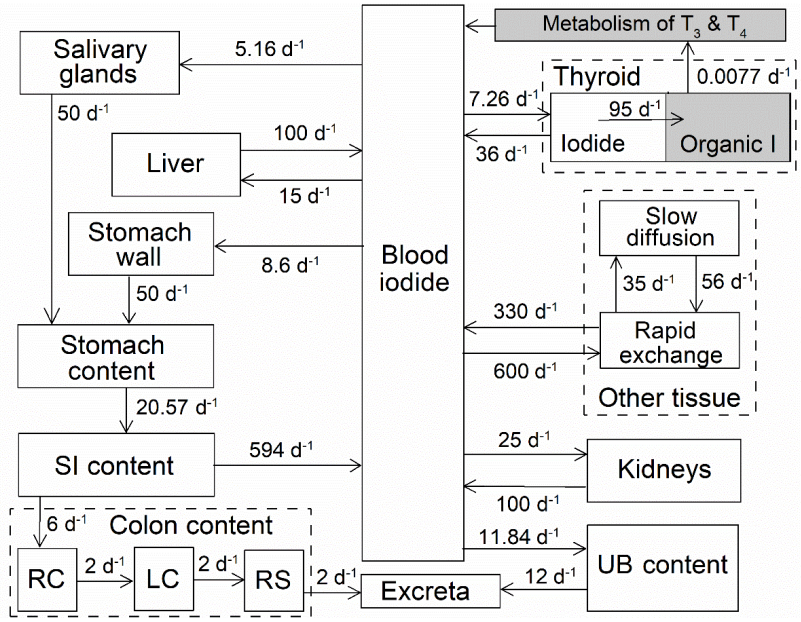

Figure 1. The ICRP's model for systemic inorganic iodide, used as a starting place for modeling the biokinetics of systemic astatine. The shaded boxes do not represent iodide kinetics but are included to show recycling of iodide over time after conversion to thyroid hormones. Flow rates shown for alimentary tract contents are values for a reference adult male in the ICRP's Human Alimentary Tract Model (ICRP 2006). Abbreviations: RC = right colon, LC = left colon, RS = rectosigmoid colon, UB = urinary bladder.

Results

Summary of biokinetic data

The biokinetics of absorbed or intravenously injected astatine resembles that of the next heaviest halogen, iodine, regarding blood clearance and excretion patterns and its selective uptake by the thyroid gland and stomach wall and high concentration in saliva. Differences in the systemic behaviors of astatine and iodine include a lower rate of loss of astatine than iodine from most

tissues and a tendency of astatine to accumulate in phagocytic tissues (i.e., tissues with relatively high levels of macrophages) such as spleen, liver, and lung (Hamilton et al., 1953; Brown, 1986; Garg et al., 1990). In a study of the toxicity of intravenously injected ^{211}At in mice, adverse effects were observed in tissues that accumulate iodine (thyroid, stomach, salivary glands) and in some phagocytic tissues at 14 and 56 d post injection (Cobb et al., 1988). The effects were more severe in phagocytic tissues, particularly the spleen, than in thyroid, stomach, and salivary glands.

Uptake and/or retention of astatine by the thyroid varied among studies, perhaps due in part to differences between species. In all studies involving comparison of astatine as astatide and iodine as inorganic iodide, accumulation of astatine in the thyroid was lower than that of iodine during the first day after administration to human subjects, monkeys, guinea pigs, rats, and mice (Hamilton et al., 1953, 1954a; Shellabarger et al., 1954; Cobb et al., 1988; Garg et al., 1990). Astatine showed longer retention than iodine in the stomach wall and in most other soft tissues (Hamilton et al., 1953; Garg et al., 1990). It has not been clearly established whether astatine becomes organically bound to some extent in the thyroid.

Following subcutaneous injection of ^{211}At and ^{131}I to guinea pigs with normal thyroids, the thyroid content and cumulative urinary and fecal excretion at 4 h represented 8.5%, 12%, and 0.8%, respectively, of the administered amount of ^{131}I, and 3.4%, 8.8%, and 0.4%, respectively, of administered ^{211}At (Hamilton and Soley, 1940). Corresponding values at 18 h were 17%, 37%, and 17% for ^{131}I and 5.4%, 36%, and 13% for ^{211}At. In a second, longer-term study involving only measurements of activity in the thyroid, the thyroid contained 9.3% of administered ^{131}I at 4 h, 18.5% at 18 h, and 18.8% at 65 h, compared with 2.9%, 7.1%, and 4.5%, of ^{211}At at 4, 18, and 65 h, respectively.

Hamilton et al. (1953) compared the biokinetics of intravenously administered ^{211}At (in sodium sulfite and sodium chloride) and ^{131}I (in sodium chloride) in rats. Plasma clearance was rapid for both radionuclides. At 24 h, plasma contained about 0.9% of injected ^{211}At and 0.6% of injected ^{131}I after correction for radioactive decay. At 1 h the thyroid and stomach wall contained, on average, 5.6% and 6.1%, respectively, of injected ^{131}I, and 1.1% and 5.2% respectively, of injected ^{211}At. The stomach content of ^{131}I decreased steadily to about 0.5% of the injected amount at 24 h, while the content of ^{211}At increased to 9.9% of the injected amount at 4 h and then decreased gradually to 5.9% at 24 h. The thyroid content of both radionuclides peaked at 24 h, at which time the thyroid contained about 1.5% of injected ^{211}At and 12% of injected ^{131}I. The ^{211}At content of the thyroid decreased by about a factor of 2 from 24-48 h and showed little if any change from 48-72 d. The ^{131}I content declined by about one-fourth from 24-72 h. Tissues other than the thyroid generally contained a larger portion of injected ^{211}At than ^{131}I from 4-24 h. The mean ^{211}At content (% injected activity) of the liver, kidneys, and muscle were, respectively, about 4.6, 5.6, and 3.6 times the content of ^{131}I. The relative selectivity S of tissues of the rat for ^{211}At compared to ^{131}I was calculated as

$$S = (\%\ ^{211}\text{At g}^{-1}\text{ tissue} / \%\ ^{211}\text{At g}^{-1}\text{ plasma}) / (\%\ ^{131}\text{I g}^{-1}\text{ tissue} / \%\ ^{131}\text{I g}^{-1}\text{ plasma})$$

Values of S were derived for 21 tissues at 1-24 h after injection of ^{211}At and ^{131}I. Values of S exceeded 1.0 (median, 7.6) for all times and tissues other than thyroid. Highest values of S

generally were seen for phagocytic tissues such as spleen and lung. Smaller values of S (median, 2.8) but still greater than 1.0 for tissues other than thyroid and urinary bladder were determined by Garg et al. (1990) at 1-24 h following intravenous (IV) administration of ^{211}At[astatide] and ^{131}I[iodide] to mice. As in the study by Hamilton et al. (1953) on rats, highest values of S were generally found for phagocytic tissues such as spleen and lung.

In studies by Hamilton et al. (1953, 1954a, 1954b), higher thyroidal accumulation of ^{211}At was observed in monkeys and human subjects than in rodents. In two monkeys, the thyroid contained 9 and 20% of administered ^{211}At at 19 h (Hamilton et al. 1953). In seven human subjects with various forms of thyroid pathology, 4.6-17.8% of administered ^{211}At was contained in the thyroid at times from 13-22 h after administration; little ^{211}At was found in the thyroid of an eighth subject (Hamilton et al. 1954a). The ^{131}I retention in these same patients was estimated as 12-30% at 24 h (Cobb et al. 1988). Hamilton and coworkers (1954a) noted an apparent correlation between ^{211}At accumulation in the thyroid and the stable iodine content of the thyroid per gram tissue in the eight human subjects.

Visser et al. (1981) compared the tissue distribution of several organic astatine compounds with that of inorganic astatine following intravenous administration to rats. They found that the organic compounds were easily dehalogenated, similarly to their iodine analogues. The time-dependent distribution of astatide was consistent with results of earlier studies on rodents including data of Hamilton and coworkers (1953, 1954a, 1954b). That is, astatide behaved similarly to iodide, accumulating in the thyroid (although to a lesser extent than iodide), stomach wall, and stomach content. The thyroid contained about 1.8% of the administered ^{211}At (correct for decay) at 15 min, 2.1% at 30 min, 2.8% at 60 min, and 3.1% at 240 min. At these times the stomach contents represented about 1.2%, 4.9%, 7.3%, and 8.1%, respectively, of the administered amount. The highest concentrations in extrathyroidal tissues over the first 6 h were found in the spleen and stomach wall, followed by lungs and kidneys (Figure 2).

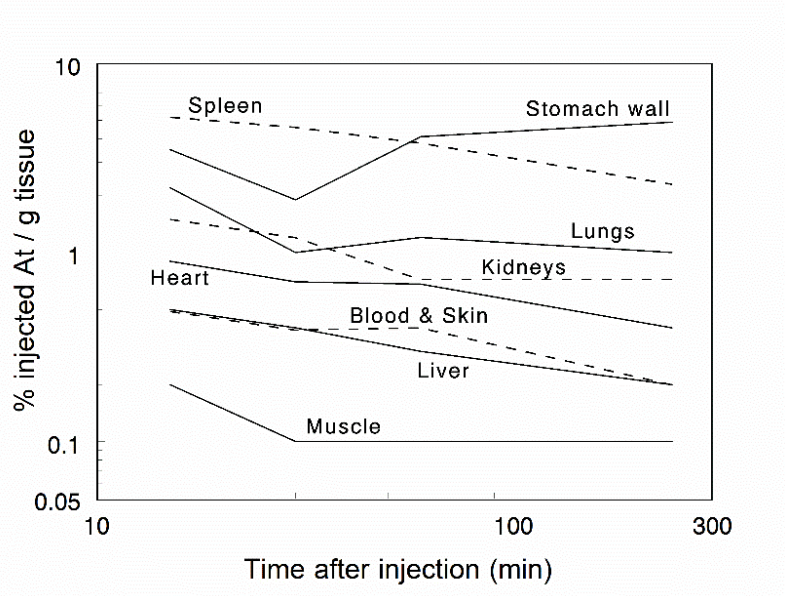

Figure 2. Time-dependent concentrations of intravenously administered ^{211}At in tissues and blood of rats (data of Visser et al., 1981).

Harrison and Royle (1984) measured the content of ^{211}At in selected tissues of mice over the first 28.5 h after IV injection. The blood content (corrected for decay) declined to ~1% of the injected amount by ~12 h post injection and remained at that level through 28.5 h. The thyroid content peaked at ~3.5% of the injected amount within 3-4 h post injection, declined to roughly 40% of the peak content by 12-15 h, and remained near that level through 28.5 h.

Larsen et al. (1998) compared the biokinetics of intravenously administered [^{131}I]iodide and [^{211}At]astatide in mice. Activity concentrations were determined in 12 tissues and in blood. High concentrations of ^{131}I were measured in thyroid and stomach at 1 and 4 h, with relatively low concentrations found in other tissues at 4 h. The thyroid also showed high concentrations of ^{211}At at 1 and 4 h but only about one-half of that of ^{131}I at 1 h and one-fourth at 4 h. The two radionuclides showed similar uptake by the stomach wall at 1 h. By 4 h the concentration of ^{131}I in the stomach had decreased considerably while the ^{211}At concentration showed little change. On average, the ^{211}At concentration in individual tissues (% dosage g^{-1}) was 3.2 (range, 2.4-4.6) times the ^{131}I concentration at 4 h with the largest concentration ratio ^{211}At:^{131}I found for spleen and lung. At 4 h, the highest ^{211}At concentrations in extrathyroidal tissues (normalized to 1.0 for kidney) decreased in the order: stomach, 13; spleen and lung, 1.6; large intestine, small intestine, and kidney, 1.0; heart, 0.81, liver, 0.77; bone, 0.48; muscle, 0.32; brain, 0.16.

Spetz et al. (2013) compared the distribution of iodide (^{125}I$^-$ and ^{131}I$^-$) and ^{211}At over the first 24 h following IV administration to rats. The activity concentration of iodide was higher than that of ^{211}At in the thyroid and lower than that of ^{211}At in all extrathyroidal tissues. Estimated absorbed doses (Gy/MBq) to tissues from ^{211}At over the first 24 h decreased in the order: thyroid, 17; stomach, 1.2; lung, 1.1; spleen, 1.0; kidney, 0.39; small intestine, 0.33; salivary glands, 0.27; large intestine, 0.21; heart, 0.18; liver, 0.16; muscle, 0.12.

The distribution of ^{209}At in mice following its IV administration as astatide was determined by *in vivo* measurement together with gamma measurement of activity in harvested tissues (Crawford 2016). At 80 min post injection the concentrations in harvested tissues (read from a bar graph and normalized to a concentration of 1.0 for stomach wall) were approximately 3.5 in neck (containing thyroid and trachea), 1.0 in stomach wall, 0.5 in lung, 0.3 in heart, 0.15 in liver, and 0.1 in blood. The total activity in the stomach wall was roughly 3 times the total activity in all other harvested tissues combined.

Ukon et al. (2020) determined the distribution of ^{211}At in mice from 5 min to 24 h post IV injection of free ^{211}At or ^{211}At-MABG. Following injection of free ^{211}At, high concentrations were seen in salivary gland, lung, stomach wall, and spleen, in addition to thyroid. Estimated absorbed doses (Gy/MBq) for mice injected with free ^{211}At decreased in the order: thyroid, 15; stomach, 5.4; lungs, 1.9; spleen, 0.65; kidneys, 0.52; testes, 0.37; small intestine, 0.34; large intestine, 0.24; heart, 0.22; liver and pancreas, 0.15; urinary bladder and skeleton, 0.094; brain, 0.037.

Cederkrantz et al. (2015) treated patients in clinical remission from recurrent ovarian cancer with intraperitoneal infusion of ^{211}At-MX35 F(ab')$_2$. Potassium perchlorate was given to block the thyroid. An estimated 10% of the administered ^{211}At escaped from the peritoneal cavity and

distributed throughout the body. Absorbed doses to tissues were estimated from blood and urine samples, gamma camera images, and single-photon emission computed tomography, coupled with preclinical data from the literature. For individual tissues for which activity concentrations presumably could be reasonably well determined from external measurement, absorbed dose estimates (mGy) from alpha particles decreased in the order: blocked thyroid, 1.8; kidney, 1.7; lung, 1.6; spleen, 1.3; heart, 1.2; liver, 0.52; red bone marrow, 0.15; breast, 0.14.

Biokinetic model for systemic astatine

The ICRP's updated biokinetic model for astatine is a variation of the ICRP's model for iodide (I^-), which, as indicated earlier, is one of three subsystems comprising the ICRP's current model for systemic iodine (ICRP 2017). The ICRP's model for the iodide subsystem is shown in Figure 1. The shaded boxes representing the other two subsystems of the ICRP's iodine model do not represent iodide kinetics but are included to show that a portion (nearly all) of the iodide that is converted to organic iodide is recycled over time to the blood iodide pool. The transfer coefficient of 7.26 d^{-1} from Blood iodide to Thyroid iodide (iodide "trapping") is the ICRP's baseline value for adults. This rate varies greatly in the population, depending largely on the level of stable iodine in diet.

The following modifications of the model structure for inorganic iodide shown in Figure 1 were made for application to astatine (Figure 3):

- The names of the two thyroid compartments were changed to Thyroid 1 and Thyroid 2, as these two compartments are used only to depict two phases of retention of astatine in the thyroid (fast removal and slow removal) rather than representing different forms of the element as in the ICRP's iodine model. Activity removed from Thyroid 2 is assigned in the astatine model to blood.
- Other tissue (all tissues and fluids not identified explicitly in the model) is represented in the astatine model as a single compartment, as it was not feasible to model different phases of retention of astatine in this region.
- Compartments representing the spleen and lungs were added to the model structure for iodide because they appear from data for laboratory animals and human subjects to be important repositories for astatine.

The following flow rates were carried over from the iodide model:

- the outflow rate from plasma (672.9 d^{-1}, rounded to four digits)
- the flow rate from plasma to urinary bladder content (11.84 d^{-1})
- the flow rates from plasma to salivary glands, stomach wall, and kidneys
- the flow rates from the rapid-turnover thyroid compartment to plasma (36 d^{-1}) and to the longer-term thyroid compartment (95 d^{-1})
- flow rates describing transfer through the alimentary tract contents, fractional absorption to blood, and fractional loss in feces

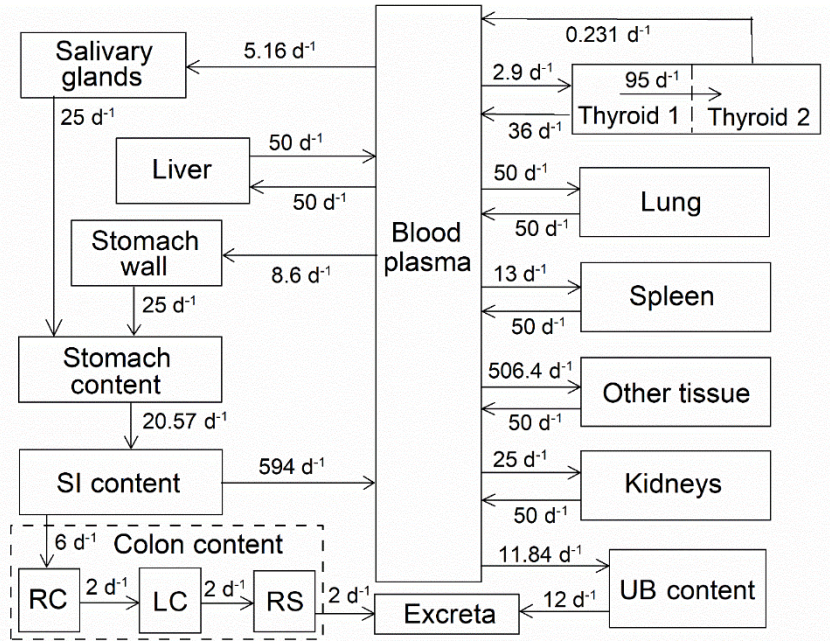

Figure 3. The ICRP's updated biokinetic model for systemic astatine. Abbreviations: RC = right colon, LC = left colon, RS = rectosigmoid colon, UB = urinary bladder.

To model the lower accumulation of astatine than iodine in the thyroid in the first day after injection of tracers into blood, the transfer rate from plasma to the rapid-turnover thyroid compartment in the iodide model was reduced by 60%, from 7.26 d^{-1} to 2.9 d^{-1}. This implies that the level of accumulation of astatine at early times (expressed as a fraction of the injected amount corrected for radioactive day) is about 40% of that of iodine. This flow rate for astatine substantially overestimates the observed accumulation of astatine in the thyroid of rats and mice but is consistent with data for guinea pigs, for which the observed ratios of thyroidal astatine to thyroidal iodine were in the range 0.3-0.4 at 4 h and 18 h. This assigned rate of uptake of astatine by the thyroid also seems consistent with the limited information on the accumulation of astatine in the thyroid in human subjects and monkeys.

Transfer from the long-term thyroid compartment directly to blood as modeled for astatine does not have an analogue in the ICRP's model for iodide. In the ICRP's full model for systemic iodine, however, organic iodine produced in the thyroid is released to a blood compartment at the rate 0.0077 d^{-1}. The rate of loss of astatine from the long-term thyroid compartment to plasma is set at a much higher value, 0.231 d^{-1}, corresponding to a biological half-time of 3 d based on the measured decline of the thyroid content in guinea pigs from 18 to 65 h after administration. This value may underestimate the residence time of astatine in the human thyroid, but dose estimates for astatine isotopes are virtually unchanged by assignment of a longer residence time due to their short physical half-lives.

Transfer rates between plasma and extrathyroidal tissues were based on the following data: relative selectivity of astatine and iodine by tissues of rats and mice; relative astatine contents of different tissues as a function of time after administration of astatine to rats and mice; and

accumulation of free ^{211}At following infusion of ^{211}At-MX35 F(ab')$_2$ (Cederkrantz et al. 2015). It was concluded from the collective data that, in the human body, the number of nuclear transformations of ^{211}At (the most frequently studied astatine isotope) per gram tissue in the activity pools identified in the model are likely to decrease in the order: Stomach wall and Salivary glands ≥ Lungs, Spleen ≥ Kidneys > Liver > Other. Although the concentration of ^{211}At in the kidneys generally was lower than that in lungs and spleen in animal studies, the model was designed to yield roughly the same astatine concentrations in kidneys as in lungs and spleen, for consistency with dose estimates for free ^{211}At in human subjects (Cederkrantz et al. 2015).

The greater accumulation of astatine than iodine in extrathyroidal tissues was modeled by reducing outflow rates depicted in the iodide model by 50%, to 25 d^{-1} for salivary glands and stomach wall and to 50 d^{-1} for liver, kidneys, and other soft tissues. A higher accumulation of astatine in the phagocytic tissues liver, lung, and spleen than in most other extrathyroidal tissues was modeled by increasing the flow rates from plasma to these tissues assumed or implied in the iodide model (lungs and spleen were implicitly contained in Other in the iodide model).

Discussion

The updated model for systemic astatine described here replaces the ICRP's astatine model introduced in Publication 30, Part 3 (1981) and modified in Publication 68 (1994) by explicit depiction of excretion pathways. That model was based on analogy with the lighter halogens chlorine (Cl) and bromine (Br). Like chlorine and bromine, astatine was assumed to leave the transfer compartment (essentially, blood) with a half-time of 6 h, distribute uniformly throughout the body, and move from tissues directly to excretion pathways with a biological half-time of 10 d. A urinary-to-fecal excretion ratio of 1 was assigned to astatine and bromine in Publication 68 (but a ratio of 100 was assigned to chlorine). The assumption of shared biokinetics was applied in Publications 30 and 68 to radioactive progeny of astatine produced in vivo. That is, radioactive progeny of astatine produced in vivo were assumed to have the same biokinetics as astatine. Essentially, shared kinetics means that the progeny do not migrate from the parent.

ICRP Publication 30 (1981) does not discuss available biokinetic studies of astatine such as those by Hamilton and co-workers (1940, 1953, 1954a, 1954b) and does not provide a rationale for assigning the model for chlorine and bromine to astatine. Presumably, assignment of a biological half-time of 10 d was considered suitably cautious for dose assessments of radioisotopes of astatine in view their short physical half-lives. In any case, the considerably larger database for astatine now available supports the conclusion of early investigators that the systemic behaviour of astatine (entering blood as astatide) is qualitatively similar to that of iodine (entering blood as iodide) but differs quantitatively from iodine in two main ways: (1) accumulation in the thyroid is lower for astatine than iodine, and (2) accumulation in non-thyroidal tissues is higher for astatine than for iodine. As described in this paper, the astatine-iodine analogy was used as the basis for the ICRP's updated systemic model for astatine, with observed differences in iodine and astatine biokinetics used to reshape the ICRP's model for systemic iodide (a sub-model of the ICRP's iodine model) into a model for systemic astatine.

The ICRP's updated model for systemic astatine was used to derive dose coefficients (Sv/Bq) for selected tissues of a reference adult male (ICRP 2002), assuming acute input of ^{210}At or ^{211}At

into blood (Table 2). Two sets of values, one showing the dose from only the parent and the other showing the dose from the full chain, were derived for each radionuclide to show the relative contributions of the parent radionuclide and its progeny to the total dose coefficient. The ICRP's current dosimetry system for workers or adult members of the public (ICRP 2015, 2016) was applied. Independent kinetics of radioactive progeny was assumed for the calculations involving progeny. That is, each chain member produced in vivo was assumed to migrate to blood at a rate that depends on the expected mobility of the element and subsequently to behave as if injected into blood as a parent radionuclide. In the ICRP's OIR series, independent kinetics is the standard treatment of radionuclides produced by radioactive decay in systemic compartments. The radioactive progeny of both ^{210}At and ^{211}At are isotopes of polonium and bismuth. Astatine-210 decays in two branches: 0.175% by alpha emission to ^{206}Bi and 99.8% by electron capture and positron emission to the alpha emitter ^{210}Po. Astatine-211 also decays in two branches: 41.8% by alpha decay to the long-lived beta-gamma emitter ^{207}Bi ($T_{1/2}$ = 32.9 y), and 58.2% by electron capture to the virtually pure alpha emitter ^{211}Po ($T_{1/2}$ = 0.516 s). In the OIR series, the assumed rates of migration of polonium and bismuth from a parent radionuclide to blood are 0.099 d^{-1} and 66.54 d^{-1}, respectively. The biokinetic models for polonium and bismuth as parent radionuclides are described in ICRP Publication 137 (2017).

As indicated in Table 2, the dose coefficients for the thyroid are considerably higher than the dose to the other addressed tissues. The dose coefficients for the stomach wall, salivary glands, lungs, spleen, and kidneys are among the highest coefficients for the 46 extrathyroidal tissues addressed in the calculations. The dose coefficients listed for muscle are reasonably representative of derived dose coefficients for most of the unlisted tissues.

Table 3 lists dose coefficients for ^{210}At and ^{211}At, corresponding to those in Table 2, based on the model for systemic astatine applied in ICRP Publication 68 (1994). Table 4 lists the ratio A:B of corresponding dose coefficients in Tables 2 and 3. The alimentary tract model and dosimetry system used to derive the values in Table 2 were also used to derive the values in Table 3, to focus on differences in dose estimates stemming from differences in the biokinetic models for systemic astatine isotopes and their progeny. For application of the model of Publication 68, systemic activity transferred to the large intestines was assigned to the right colon content in the HATM, and shared kinetics of progeny was assumed. Thus, polonium and bismuth isotopes produced in systemic compartments by decay of ^{210}At or ^{211}At were assumed to be uniformly distributed in tissues and removed to excretion pathways with a biological half-time of 10 d.

Table 2. Dose coefficients (Sv/Bq) for injection of ^{210}At or ^{211}At into blood of an adult male, based on the updated model for systemic astatine described in this paper.				
	^{210}At		^{211}At	
Tissue	Parent only	Progeny included	Parent only	Progeny included
Thyroid	4.41E-09	7.39E-08	5.27E-07	1.46E-06
Stomach wall	3.62E-10	4.28E-09	2.44E-08	6.75E-08
Salivary glands	2.96E-10	7.71E-09	3.13E-08	8.66E-08
Lungs	2.31E-10	4.59E-09	1.73E-08	4.65E-08
Spleen	2.71E-10	1.00E-08	1.69E-08	4.67E-08
Kidneys	2.61E-10	1.84E-08	1.74E-08	4.80E-08
Urinary bladder wall	2.45E-10	9.89E-10	2.40E-09	6.74E-09
Liver	1.71E-10	1.20E-08	6.58E-09	1.82E-08
Red marrow	1.13E-10	2.46E-09	2.18E-09	6.21E-09
Muscle	7.18E-11	8.19E-10	2.26E-09	6.25E-09

As seen in both Table 2 (containing values based on the updated model) and Table 3 (containing values based on the Publication 68 model), the doses delivered by the radioactive progeny are greater than the doses deliver by the parent radionuclide, particularly for ^{210}At. As seen in Table 3, the doses from the full ^{210}At or ^{211}At chain based on the Publication 68 model are somewhat uniform across tissues. This is due to the ingrowth of the long-lived alpha emitter ^{210}Po, which delivers a much greater dose than ^{210}At, and the assumption that the progeny remains with its uniformly distributed parent. The somewhat uniform distribution of doses from the ^{210}At chain based on the Publication 68 model contrasts with the more nonuniform values in Table 2, which reflect the redistribution of ingrowing ^{210}Po implied by the assumption of independent kinetics of progeny and the highly non-uniform distribution of activity predicted by the systemic model for polonium (ICRP 2017). Some degree of non-uniformity of estimated doses even for values based on the Publication 68 models result from the assumed contribution of activity in blood to tissue doses in the ICRP's current dosimetry system. That system depicts a reasonably realistic, highly nonuniform distribution of blood in the human body.

As indicated by the dose ratios in Table 4, dose coefficients for the thyroid based on the updated model are far greater than those based on the Publication 68 model. Dose coefficients based on the updated model are also generally much greater than those based on the Publication 68 model for the other two important iodide repositories addressed in Tables 2-4 (stomach wall and salivary glands), for two of the three phagocytic tissues addressed (lungs and spleen), and for kidneys. For the other phagocytic tissue, liver, the dose coefficient based on the updated model is greater than that based on the Publication 68 model only for the case in which the full ^{210}At chain is addressed. In this case, the much greater dose to liver based on the updated model results from the assumption of independent kinetics of progeny. This assumption allows a reasonably realistic

depiction of the migration of the ^{210}At progeny ^{210}Po to the liver, which is known to be an important repository for internally deposited polonium.

Table 3. Dose coefficients (Sv/Bq) for injection of ^{210}At or ^{211}At into blood of an adult male based on the biokinetic model for systemic astatine applied in ICRP Publication 68

	^{210}At		^{211}At	
Tissue	Parent only	Progeny included	Parent only	Progeny included
Thyroid	1.27E-10	7.63E-10	5.56E-09	1.54E-08
Stomach wall	1.83E-10	7.66E-10	7.40E-09	2.05E-08
Salivary glands	6.83E-11	7.66E-10	3.38E-09	9.35E-09
Lungs	1.96E-10	6.56E-10	9.19E-09	2.53E-08
Spleen	1.88E-10	6.99E-10	9.94E-09	2.75E-08
Kidneys	1.81E-10	7.41E-10	8.22E-09	2.27E-08
Urinary bladder wall	1.11E-10	8.24E-10	2.89E-09	7.99E-09
Liver	1.90E-10	7.67E-10	7.61E-09	2.10E-08
Red marrow	2.36E-10	8.10E-10	5.79E-09	1.62E-08
Muscle	8.86E-11	7.98E-10	2.98E-09	8.24E-09

Table 4. Ratio A:B of dose coefficients (DCs) for injection of ^{210}At or ^{211}At in blood of an adult male, where A is the dose coefficient based on the updated astatine model described in this paper and B is the dose coefficient based on the Publication 68 model

	^{210}At		^{211}At	
Tissue	DCs based on parent only	DCs based on full chain	DCs based on parent only	DCs based on full chain
Thyroid	35	97	95	95
Stomach wall	2.0	5.6	3.3	3.3
Salivary glands	4.3	10	9.3	9.3
Lungs	1.2	7.0	1.9	1.8
Spleen	1.4	14	1.7	1.7
Kidneys	1.4	25	2.1	2.1
Urinary bladder wall	2.2	1.2	0.83	0.84
Liver	0.90	16	0.87	0.87
Red marrow	0.48	3.0	0.38	0.38
Muscle	0.81	1.0	0.76	0.76

References

Brown I. 1986. Astatine-211: its possible applications in cancer therapy. Int. J. Radiat. Appl. Instrum. Part A. Appl. Radiat. Isot. **37** 789-98.

Cobb LM, Harrison A and Butler SA. 1988. Toxicity of ^{211}At in the mouse. Human Toxicol. **7** 529-534.

Cederkrantz E et al. 2015. Absorbed doses and risk estimates of ^{211}At-MX35 F(ab')$_2$ in intraperitoneal therapy of ovarian cancer patients. Int. J. Radiat. Oncol. Biol. Phys. **93** 569-576.

Crawford J. 2016. New technologies for ^{211}At targeted α-therapy research using ^{211}Rn and ^{209}At. [doctoral dissertation] University of Victoria.

Garg PK, Harrison CL and Zalutsky MR. 1990. Comparative tissue distribution in mice of the α-emitter 211At and 131I as labels of monoclonal antibody and F(ab')2 fragment. Cancer Res. **50** 3514-3520.

Hamilton JG, Asling CW, Garrison WM and Scott KG. 1953. The accumulation, metabolism and biological effects of astatine in rats and monkeys. University of California Publications in Pharmacology **2** 283-343.

Hamilton JG, Durbin PW and Parrott MW. 1954a. Accumulation of ^{211}Astatine by thyroid gland in man. Exptl. Biol. Med. **86** 366-369.

Hamilton JG, Durbin PW and Parrott M. 1954b. The accumulation and destructive action of astatine-211 (eka-iodine) in the thyroid gland of rats and monkeys. J. Clin. Endocrin. Metab. **14** 1161-1178.

Hamilton JG and Soley MH. 1940. A comparison of the metabolism of iodine and of element 85 (Eka-iodine). Proc. N. A. S. **26** 483-489.

Harrison A and Royle L. 1984. Determination of absorbed dose to blood, kidneys, testes and thyroid in mice injected with ^{211}At and comparison of testes mass and sperm number in X-irradiated and ^{211}At treated mice. Health Phys. **46** 377-383.

ICRP. 1981. Limits for Intakes of Radionuclides by Workers. ICRP Publication 30 (Part 3). Ann. ICRP **6** (2-3).

ICRP, 1994. Dose Coefficients for Intakes of Radionuclides by Workers. ICRP Publication 68. Ann. ICRP **24** (4).

ICRP. 2002. Basic Anatomical and Physiological Data for Use in Radiological Protection Reference Values. ICRP Publication 89. Ann. ICRP **32** (3-4).

ICRP. 2006. Human Alimentary Tract Model for Radiological Protection. ICRP Publication 100. Ann ICRP **36** (1-2).

ICRP. 2008. Nuclear Decay Data for Dosimetric Calculations. ICRP Publication 107. Ann ICRP **38** (3).

ICRP. 2015. Occupational Intakes of Radionuclides: Part 1. ICRP Publication 130 Ann. ICRP **44**.

ICRP. 2016. The ICRP computational framework for internal dose assessment for reference adults: specific absorbed fractions. ICRP Publication 133 Ann. ICRP **45**

ICRP. 2017. Occupational intakes of radionuclides: Part 3. ICRP Publication 137. Ann. ICRP **46**(3/4).

ICRP. In press. Occupational intakes of radionuclides: Part 5.

Larsen RH, Slade S and Zalutsky MR. 1998. Blocking [^{211}At]astatide accumulation in normal tissues: preliminary evaluation of seven potential compounds. Nucl. Med. Biol. **25** 351-357.

Lindegren S, Albertsson P, Back T, Jensen H, Palm S and Aneheim E. 2020. Realizing clinical trials with astatine-211: the chemistry infrastructure. Cancer Biother. Radiopharm. **35** 425-436.

Shellabarger CJ and Godwin JT. 1954. Studies of the thyroidal uptake of astatine in the rat. J. Clin. Endocrin. Metab. **14** 1149-1160.

Spetz J, Rudqvist N and Forssell-Aronsson E. 2013. Biodistribution and dosimetry of free ^{211}At, $^{125}I^-$ and $^{131}I^-$ in rats. Cancer biotherapy and radiopharmaceuticals **28** 657-664.

Ukon N, Zhao S, Washiyama K, Oriuchi N, Tan C, Shimoyama S, Aoki M, Kubo H, Takahashi K and Ito H. 2020. Human dosimetry of free ^{211}At and meta-[^{211}At]astatobenzylguanidine (^{211}At-MABG) estimated using preclinical biodistribution from normal mice. EJNMMI Physics. https://doi.org/10.1186/s40658-020-00326-7.

Vaidyanathan G and Zalutsky M R. 2008. Astatine radiopharmaceuticals: prospects and problems. Curr. Radiopharm. **1** 177.

Visser GWM, Visser EL, Diemer CM, Vos FM and Kaspersen T. 1981.The biological behaviour of some organic astatine compounds in rats. Int. J. Appl. Radiat.Isotop **32** 81-85**.**

Wilbur D S. 2013. Enigmatic astatine. Nature Chemistry 5:246.